

Gradient-free online learning of subgrid-scale dynamics with neural emulators

Hugo Frezat,^{1, 2, 3, *} Ronan Fablet,³ Guillaume Balarac,^{1, 4} and Julien Le Sommer²

¹*Université Grenoble-Alpes, LEGI, Grenoble, France*

²*Université Grenoble-Alpes, IGE, Grenoble, France*

³*Inria team Odyssey, Brest, France*

⁴*Institut Universitaire de France (IUF), Paris, France*

(Dated: October 2023)

In this paper, we propose a generic algorithm to train machine learning-based subgrid parametrizations online, i.e., with *a posteriori* loss functions for non-differentiable numerical solvers. The proposed approach leverage neural emulators to train an approximation of the reduced state-space solver, which is then used to allows gradient propagation through temporal integration steps. The algorithm is able to recover most of the benefit of online strategies without having to compute the gradient of the original solver. It is demonstrated that training the neural emulator and parametrization components separately with respective loss quantities is necessary in order to minimize the propagation of some approximation bias.

I. INTRODUCTION

Numerical models used for simulating the evolution of fluid flows generally require subgrid scales (SGS) and physical parameterizations. These serve the purpose of representing the impact of scales that remain unresolved by the discretized solver as for instance subgrid turbulent processes [1, 2]. They may also account for other physical phenomena that are not explicitly accounted for by the partial differential equations. SGS and physical parameterizations are generally considered to be key components of numerical models in Earth System science [3, 4]. In these numerical models, they are often rate-controlling components which largely govern the long term behavior of model solutions [5, 6]. This is why significant efforts are concentrated on the development of SGS and physical parameterizations in these communities. Machine learning (ML) techniques have now been widely applied to SGS and physical parameterizations for numerical simulations, as already discussed in reviews [7, 8]. These ML-based components have been demonstrated in different applications, including atmospheric circulation [9], oceanic circulation [10], and magnetohydrodynamics models [11]. The ambition of this emerging field is to design hybrid numerical models that improves upon existing ones by combining physics-based PDE solvers and ML-based trainable components. In this framework, well-constrained aspects are incorporated into the resolved equations, while components that are less rigorously constrained or follow a statistical behavior are represented by ML-based algorithms. When possible, physical knowledge can also be incorporated in the ML-based component [12–14]. Hybrid numerical models are currently designed through an optimization procedure that attempts to improve its ability to replicate the results of a higher resolution model. The hybrid numerical models are typically run

at coarser resolution and the parameters of their ML components are optimized in order to fit a given training objective. This objective is usually formulated from pre-existing high-resolution, process resolving numerical models (that is direct numerical simulation (DNS), or high-resolution version of the same code) but also in principle be formulated from observations or lab experiments. By essence, this optimization is very much related to the tuning of model parameters, or to the estimation of state-dependent correction of models.

Several recent results suggest that ML-based SGS parametrization give better results when the ML components are trained with online strategies [15–19]. The training of ML components for hybrid numerical models is said to use an online strategy if the evaluation of the training objective involves integrating the hybrid numerical model for several time steps. Note that the same idea has also been referred to as *a posteriori* [20], solver-in-the-loop [21], differentiable [22, 23] or end-to-end in the ML community. In practice, the strategy has been shown to lead to more stable simulations, with better performance in *a posteriori* tests. However, the online strategy typically requires to compute the derivative of the hybrid numerical model with respect to the parameters of the ML components. These results suggest that, as in other fields of physical science, the emerging paradigm of differentiable programming shows great potential for the design of hybrid numerical models applied to the simulations of turbulent systems. Differentiable programming (DP) is often combined with automatic differentiation (AD) which allows to automatically obtain the derivatives of a chain of operations in order to be used in an optimization procedure based on a gradient descent variant. AD frameworks are typically implemented by specific libraries or programming languages, and have seen many new development applications in physical sciences [24–27]. There has been a particularly active community around the problem of turbulence modeling [28–30] and climate-geoscientific modeling [31–33].

* <https://hrkz.github.io>; hugo.frezat@gmail.com

However, most numerical models are usually not easily differentiable. This major practical issue makes the optimization of ML components with online strategies difficult. For performance and historic reasons, legacy codes used in production are written in Fortran or C programming languages, with relatively low abstraction levels. This is the case in many physics community including for Earth System models used for climate projections. These hand-optimized numerical models are also relatively large codebases (hundreds of thousands of lines of codes) and would thus require lots of effort to be re-implemented in a modern AD language. Generating adjoints automatically using code analysis libraries is possible, but practically complicated to deploy and lead to suboptimal codes (in particular in terms of memory footprint). In practice, online learning strategies are thus not easily amenable with production scale codes. Different approaches that includes the temporal aspect provided by online learning have also been proposed and rely on gradient-free optimization algorithms. While gradient-free optimization is a large subfield, we identify two large families that have recently seen many applications to training large ML models in the context of hybrid physical models. First, methods adapted from data assimilation [34, 35] and inverse problems as for instance the ensemble kalman inversion (EKI) [36–38]. More recently, many studies applying gradient-free policy search in reinforcement learning (RL) have been explored in particular for turbulence modeling [39–42]. Overall, it is not clear whether which strategy performs best or should be preferred in practical situations.

Alternatively, we here propose to leverage neural emulation as a strategy to perform online supervised learning while avoiding the need for a differentiable solver. The use of neural emulators also connects with some algorithms in the field of simulation based inference which use neural networks to solve inverse problems [43] and the field of data assimilation for model error correction [44, 45]. Here, the neural emulator aims at approximating the full solver in the (reduced) model state space. We can rephrase the neural emulation as an approximation of the temporal evolution of some PDE. We describe in this paper a generic algorithm which allows to train jointly a ML-based SGS parametrization for a non-differentiable solver with an online strategy and a neural emulator of the same solver. To overcome bias separation between the two components, we introduce a two-step procedure and a compensated loss function that isolates the different training objectives. The algorithm is implemented and demonstrated to produce stable models on a challenging subgrid parametrization problem. We also show that we are able to recover most of the benefits of online strategies without having to compute the gradient of the reduced resolution solver.

The paper is structured as follows: in Section 2, we

outline the general issue being addressed and its particular application to SGS modeling. Section 3 describes the two-step algorithm that allows training a SGS parametrization with online strategy using a differentiable neural emulator of the target solver. In Section 4, we describe our evaluation benchmark, consisting of a two-dimensional quasi-geostrophic system subject to kinetic energy backscatter. The performance of our approach is then illustrated in Section 5 and discussed in Section 6.

II. PROBLEM STATEMENT

As explained in the introduction, training a model online requires the ability to compute the gradient of the loss function w.r.t. model parameters, which involves solver calls and consequently also requires its gradient. Let us define a typical regression task where one would seek to minimize a cost between some prediction $\hat{\mathbf{z}} = \mathcal{M}(\mathbf{y} | \theta)$ and ground truth of the same input space \mathbf{z} , i.e.

$$\arg \min_{\theta} \mathcal{L}(\mathbf{z}, \mathcal{M}(\mathbf{y} | \theta)). \quad (1)$$

During the training process, the parameters of \mathcal{M}, θ are optimized in order to minimize \mathcal{L} . The minimization algorithm requires the computation of the gradient of the loss function w.r.t. the trainable parameters θ ,

$$\frac{\partial \mathcal{L}}{\partial \theta}(\mathbf{z}, \mathcal{M}(\mathbf{y} | \theta)) = \frac{\partial \mathcal{M}}{\partial \theta}(\mathbf{y} | \theta) \frac{\partial \mathcal{L}}{\partial \mathcal{M}}. \quad (2)$$

In practice, \mathcal{M} could be a simple operator from which the analytical gradient would be computed beforehand and provided to the optimization process. However, in differentiable solvers, we are interested in the temporal evolution of a system $E(\mathbf{y}) : \mathbb{R}^n \rightarrow \mathbb{R}^n$ of a vector-valued quantity of interest $\mathbf{y}(t)$. In a discretized formulation, the operator E is typically defined by a sequence of operations,

$$\mathbf{y}(t + \Delta t) = E_m \circ \cdots \circ E_1(\mathbf{y}(t)). \quad (3)$$

Now, if $\mathcal{M} \equiv E$, the required partial derivative of the system is defined as a Jacobian in the minimization formulation (2),

$$\frac{\partial E_i}{\partial \theta} = \begin{bmatrix} \frac{\partial E_{i,1}}{\partial \theta_1} & \cdots & \frac{\partial E_{i,1}}{\partial \theta_n} \\ \vdots & \ddots & \vdots \\ \frac{\partial E_{i,n}}{\partial \theta_1} & \cdots & \frac{\partial E_{i,n}}{\partial \theta_n} \end{bmatrix} \quad (4)$$

for a single step of the temporal evolution operator E . Composing the partial derivatives of the sequences of operators in E can be done by applying the chain rule,

$$\frac{\partial E}{\partial \theta} = \frac{\partial(E_m \circ \cdots \circ E_1)}{\partial \theta} = \frac{\partial E_m}{\partial E_{m-1}} \cdots \frac{\partial E_2}{\partial E_1} \frac{\partial E_1}{\partial \theta} \quad (5)$$

The gradient of E can quickly become difficult to maintain by hand. Note that when training NNs, it is required to have a scalar-valued loss function \mathcal{L} , which means that its derivative is a gradient instead of a Jacobian. The way partial derivatives are computed is called reverse-mode differentiation [46], which here consists of a series of matrix-vector multiplications starting from

$$\frac{\partial E_1}{\partial \theta} \frac{\partial \mathcal{L}}{\partial \mathcal{M}} : \mathbb{R}^{m \times n} \rightarrow \mathbb{R}^m. \quad (6)$$

Solving (5) can be as trivial as implementing a solver leveraging automatic differentiation (AD) languages or libraries. However, as pointed out in the introduction, this is a challenging task for large-scale solvers such as GCMs that would require a lot of development work and might lead to the vanishing gradient problem [47] due to many function compositions.

II.1. The specific SGS modeling problem

Here, we are interested in modeling small-scale quantities arising in differential equations restricting the grid resolution and thus the performance of the simulations [48]. We assume an underlying differential equation involving the time evolution of variables $\mathbf{y}(t)$ to be known and defined by a direct operator $f(\mathbf{y})$. The aim is to solve an equivalent approximation for reduced variables $\bar{\mathbf{y}}(t)$ such that

$$\begin{cases} \frac{\partial \mathbf{y}}{\partial t} = f(\mathbf{y}), & \mathbf{y} \in \Omega \\ \frac{\partial \bar{\mathbf{y}}}{\partial t} = g(\bar{\mathbf{y}}) + \mathcal{M}(\bar{\mathbf{y}}), & \bar{\mathbf{y}} \in \bar{\Omega} \\ \mathcal{T}(\mathbf{y}) = \bar{\mathbf{y}} \end{cases} \quad (7)$$

where $\bar{\Omega} \subset \Omega$, g a reduced operator, \mathcal{M} a SGS model and \mathcal{T} a projection that maps direct variables to reduced ones. The objective is formulated as an inverse problem where operator \mathcal{M} has to be determined such that the evolution of the reduced variables match the projection $\mathcal{T}(\mathbf{y})$ of the direct variables \mathbf{y} . In most situations, we have $f = g$ with variables existing on different spaces or dimensionalities. Note that this can be applied to any type of partial differential equation without any loss of generality. Within a learning framework, one states the identification of a general reduced term

$$\tau(\mathbf{y}) = \mathcal{T}(f(\mathbf{y})) - g(\mathcal{T}(\mathbf{y})) \approx \mathcal{M}(\bar{\mathbf{y}} | \theta) \quad (8)$$

where θ are trainable model parameters. Under the assumption that \mathcal{T} commutes with partial derivatives, the classical approach comes to train a model $\mathcal{M}(\bar{\mathbf{y}} | \theta)$ as a functional approximation of the missing term $\tau(\mathbf{y})$. The classical strategy to optimize \mathcal{M} is to generate a dataset $\mathbb{D} = \{\bar{\mathbf{y}}\} \rightarrow \{\tau(\mathbf{y})\}$ that maps input states $\bar{\mathbf{y}}$ to the SGS term $\tau(\mathbf{y})$ beforehand and then finding optimal parameters θ offline, i.e., without any knowledge of the dynamics

$\partial \bar{\mathbf{y}} / \partial t$. Here, let us refer to an offline loss $\mathcal{L}_<$, the corresponding minimization problem (1) writes

$$\arg \min_{\theta} \mathcal{L}_< = \arg \min_{\theta} \ell_<(\tau(\mathbf{y}), \mathcal{M}(\bar{\mathbf{y}} | \theta)) \quad (9)$$

where $\ell_<$ is an instantaneous scalar-valued loss function $\ell_< : (\mathbb{R}^n, \mathbb{R}^n) \rightarrow \mathbb{R}$. In this context, \mathcal{M} is defined as a NN implemented in a standard deep learning framework such as Pytorch or TensorFlow. This allows for the computation of the gradient of the loss function, i.e., injecting (9) in (2),

$$\frac{\partial \mathcal{L}_<}{\partial \theta} = \frac{\partial \ell_<}{\partial \mathcal{M}} \frac{\partial \mathcal{M}}{\partial \theta}(\bar{\mathbf{y}} | \theta). \quad (10)$$

Using this formulation, the problem is simple to setup since both terms on the r.h.s. are automatically determined using AD capabilities. However, while the offline approach is efficient to accurately reproduces the statistical properties of the missing term $\tau(\mathbf{y})$, it has been shown to lead to unstable simulations in non-linear, chaotic dynamical systems such as those found in turbulence modeling [49]. Improving the stability of the SGS model can be done by increasing the size of the dataset, in particular by reducing the inter-sample correlation [50] or adding physics-based terms in the loss function [51]. As pointed out in [20], the offline training approach may not be able to optimize a model based on relevant metrics in the context of a dynamical system. An equivalent training approach tailored to this task, called online, has already been explored successfully in turbulence modeling [19, 24, 25]. Formally, [20] described the minimization problem (1) of the online loss $\mathcal{L}_>$,

$$\arg \min_{\theta} \mathcal{L}_> = \arg \min_{\theta} \ell_>(\{\mathbf{y}(t)\}_{t \in [t_0, t_1]}, \{\Phi_{\theta}^t(\bar{\mathbf{y}}(t_0))\}_{t \in [t_0, t_1]}) \quad (11)$$

where Φ is the flow operator that advances the reduced variables in time using the currently training model \mathcal{M} ,

$$\Phi_{\theta}^t(\bar{\mathbf{y}}(t_0)) = \bar{\mathbf{y}}(t_0) + \int_{t_0}^t g(\bar{\mathbf{y}}(t')) + \mathcal{M}(\bar{\mathbf{y}}(t') | \theta) dt' \quad (12)$$

and $\ell_>$ is a temporal scalar-valued loss function $\ell_> : (\mathbb{R}^{n \times M}, \mathbb{R}^{n \times M}) \rightarrow \mathbb{R}$ defined on M timesteps that discretizes the temporal interval $[t_0, t_1]$. Let us expand the gradient of the online loss $\mathcal{L}_>$ from (2) at final time t_1 ,

$$\frac{\partial \mathcal{L}_>}{\partial \theta} = \frac{\partial \ell_>}{\partial \Phi_{\theta}^t} \frac{\partial \Phi_{\theta}^t}{\partial \theta}(\bar{\mathbf{y}}(t_0)) = \frac{\partial \ell_>}{\partial \Phi_{\theta}^t} \left(\int_{t_0}^t \frac{\partial g(\bar{\mathbf{y}}(t'))}{\partial \theta} + \frac{\partial \mathcal{M}(\bar{\mathbf{y}}(t') | \theta)}{\partial \theta} dt' \right). \quad (13)$$

This process requires the ability to compute the partial derivatives of the reduced solver g w.r.t. the trained model parameters θ , i.e. $\partial g / \partial \theta$. Here we are interested in determining this quantity such that τ can be learnt online without re-implementing g using an AD framework.

III. COUPLED SGS-EMULATION

Building on [45], we propose an algorithm that is able to jointly train a differentiable emulator of g and its cor-

responding SGS term. Let us introduce a differentiable emulator \mathcal{E} of g

$$\mathcal{E}(\bar{\mathbf{y}}) \approx g(\bar{\mathbf{y}}), \text{ s.t. } \frac{\partial \mathcal{E}}{\partial \theta} \text{ is known.} \quad (14)$$

This differentiability condition is automatically fulfilled if \mathcal{E} is implemented using AD capabilities. It is possible to define \mathcal{E} as a trainable neural emulator, which involves training its parameters Θ simultaneously with the SGS model parameters θ . Substituting into (11),

$$\arg \min_{\Theta, \theta} \ell_>(\{\mathbf{y}(t)\}_{t \in [t_0, t_1]}, \{\varphi_{\Theta, \theta}^t(\bar{\mathbf{y}}(t_0))\}_{t \in [t_0, t_1]}) \quad (15)$$

where the coupled flow operator that jointly learns parameters Θ and θ is given by

$$\varphi_{\Theta, \theta}^t(\bar{\mathbf{y}}(t_0)) = \bar{\mathbf{y}}(t_0) + \int_{t_0}^t \mathcal{E}(\bar{\mathbf{y}}(t') | \Theta) + \mathcal{M}(\bar{\mathbf{y}}(t') | \theta) dt'. \quad (16)$$

We recall here that the final goal of this algorithm is to provide a stable SGS model \mathcal{M} that will be used for forward simulations with the reduced solver g . However, with the coupled formulation (15), the model \mathcal{M} is not explicitly restricted to represent SGS dynamics only. Indeed the algorithm jointly optimizes Θ and θ such that $\mathcal{E} + \mathcal{M}$ approximates the direct solver f . There is therefore no guarantee that θ will be optimal for \mathcal{M} to represent the SGS term.

III.1. Joint neural SGS-emulation learning

It is possible to penalize both the neural emulator and the SGS model by composing the loss function such that $\ell = \ell_{\mathcal{E}}(\mathcal{E}(\bar{\mathbf{y}} | \Theta)) + \ell_{\mathcal{M}}(\mathcal{M}(\bar{\mathbf{y}} | \theta))$ using filtering operations but their respective definitions may not be simple to implement and might not include inter-scale transfers. Instead, we propose a two-step online formulation that trains \mathcal{E} and \mathcal{M} sequentially,

Step 1 (emulator):

$$\arg \min_{\Theta} \ell_>^{\mathcal{E}}(\{\bar{\mathbf{y}}(t)\}_{t \in [t_0, t_1]}, \{\varphi_{\Theta}^t(\bar{\mathbf{y}}(t_0))\}_{t \in [t_0, t_1]}), \quad (17)$$

Step 2 (model):

$$\arg \min_{\theta} \ell_>^{\mathcal{M}}(\{\mathbf{y}(t)\}_{t \in [t_0, t_1]}, \{\varphi_{\theta}^t(\bar{\mathbf{y}}(t_0))\}_{t \in [t_0, t_1]}). \quad (18)$$

These two steps are formulated using an online learning strategy, but (17) minimizes a loss for an integration of the reduced solver g while (18) is equivalent to the classical online SGS formulation (11) with $\mathcal{E} \approx g$. Using these sequential steps, it is straightforward to show that a differentiable version of the reduced solver is not required. Indeed, let us factor the modified flows φ appearing on

the right-hand side of (17) and (18) respectively,

$$\varphi_{\Theta}^t(\bar{\mathbf{y}}(t_0)) = \bar{\mathbf{y}}(t_0) + \int_{t_0}^t \mathcal{E}(\bar{\mathbf{y}}(t') | \Theta) dt', \quad (19)$$

$$\varphi_{\theta}^t(\bar{\mathbf{y}}(t_0)) = \bar{\mathbf{y}}(t_0) + \int_{t_0}^t \mathcal{E}(\bar{\mathbf{y}}(t')) + \mathcal{M}(\bar{\mathbf{y}}(t') | \theta) dt'. \quad (20)$$

Then, expanding again the gradient of the online losses using (2) yields,

$$\frac{\partial \ell_>^{\mathcal{E}}}{\partial \varphi_{\Theta}^t} \frac{\partial \varphi_{\Theta}^t}{\partial \Theta}(\bar{\mathbf{y}}(t_0)) = \frac{\partial \ell_>^{\mathcal{E}}}{\partial \varphi_{\Theta}^t} \left(\int_{t_0}^t \frac{\partial \mathcal{E}(\bar{\mathbf{y}}(t'))}{\partial \Theta} dt' \right), \quad (21)$$

$$\frac{\partial \ell_>^{\mathcal{M}}}{\partial \varphi_{\theta}^t} \frac{\partial \varphi_{\theta}^t}{\partial \theta}(\bar{\mathbf{y}}(t_0)) = \frac{\partial \ell_>^{\mathcal{M}}}{\partial \varphi_{\theta}^t} \left(\int_{t_0}^t \frac{\partial \mathcal{E}(\bar{\mathbf{y}}(t'))}{\partial \theta} + \frac{\partial \mathcal{M}(\bar{\mathbf{y}}(t') | \theta)}{\partial \theta} dt' \right) \quad (22)$$

with \mathcal{E}, \mathcal{M} are arbitrary NNs implemented using AD and $\ell_>^{\mathcal{E}}, \ell_>^{\mathcal{M}}$ loss functions also defined within the machine learning framework, supporting AD by construction.

III.2. Neural emulator error compensations

We know that in theory, the two-step algorithm would be equivalent to the classical online SGS learning scheme with a differentiable solver if and only if $\mathcal{E} \equiv g$. In practice however, the neural emulator will only represent an approximation of the reduced solver, i.e., $\mathcal{E} \approx g$. The performance of the SGS training (18) thus strongly relies on the emulator's ability to reproduce the reduced dynamics on a given horizon $[t_0, t]$. The instantaneous emulation mismatch between the differentiable solver and the differentiable solver can be expressed as

$$\varepsilon(\bar{\mathbf{y}}) = g(\bar{\mathbf{y}}) - \mathcal{E}(\bar{\mathbf{y}}). \quad (23)$$

Substituting in the two-step SGS training (18) with the reduced solver on the left-hand side and the emulation mismatch on the right-hand side, we obtain

$$\begin{aligned} \ell_>^{\mathcal{M}}(\{\mathbf{y}(t)\}_{t \in [t_0, t_1]}, \{\varphi_{\theta}^t(\bar{\mathbf{y}}(t_0))\}_{t \in [t_0, t_1]}) \\ = \ell_>^{\mathcal{M}}(\{\mathbf{y}(t_0) + \int_{t_0}^t f(\mathbf{y}(t')) dt'\}_{t \in [t_0, t_1]}, \\ \{\bar{\mathbf{y}}(t_0) + \int_{t_0}^t \mathcal{E}(\bar{\mathbf{y}}(t')) + \mathcal{M}(\bar{\mathbf{y}}(t') | \theta) dt'\}_{t \in [t_0, t_1]}) \\ = \ell_>^{\mathcal{M}}(\{\bar{\mathbf{y}}(t_0) + \int_{t_0}^t g(\bar{\mathbf{y}}(t')) + \tau(\mathbf{y}(t')) dt'\}_{t \in [t_0, t_1]}, \\ \{\bar{\mathbf{y}}(t_0) + \int_{t_0}^t g(\bar{\mathbf{y}}(t')) + \mathcal{M}(\bar{\mathbf{y}}(t') | \theta) - \varepsilon(\bar{\mathbf{y}}(t')) dt'\}_{t \in [t_0, t_1]}). \end{aligned} \quad (24)$$

It is clear here that the emulation mismatch ε will be absorbed by the SGS model \mathcal{M} during its training phase, since \mathcal{E} is already fixed. In order to optimize \mathcal{M} against

τ using this standard online loss function, it is important that the emulation mismatch remain small. Controlling this mismatch is challenging in particular due to the temporal integration. Recall that the loss function $\ell_{>}^{\mathcal{M}}$ is defined on a sequence of states of the system $\bar{\mathbf{y}}(t)$ but never involves the missing SGS term τ that \mathcal{M} is trying to learn. As a conservative solution, we propose to transform the loss function $\ell_{>}^{\mathcal{M}}$ so that it operates on the SGS term of the temporal states,

$$\begin{aligned} \ell_{>}^{\mathcal{M}_c}(\{\mathbf{y}(t)\}_{t \in [t_0, t_1]}, \{\varphi_{\theta}^t(\bar{\mathbf{y}}(t_0))\}_{t \in [t_0, t_1]}) \\ = \ell_{>}^{\mathcal{M}}(\{\tau(\mathbf{y}(t))\}_{t \in [t_0, t_1]}, \{\mathcal{M}(\varphi_{\theta}^t(\bar{\mathbf{y}}(t_0)))\}_{t \in [t_0, t_1]}). \end{aligned} \quad (25)$$

Penalizing these terms in the loss function removes any ambiguities w.r.t. the emulation mismatch ε while maintaining the online behavior of the learning strategy, since these quantities are still evaluated over a temporal horizon $[t_0, t]$. The discretized version of the two-step algorithm, suitable for numerical applications (detailed below), is outlined in Algorithm 1.

IV. APPLICATION: QUASI-GEOSTROPHIC DYNAMICS

In turbulent flows, the energy cascade drives energy from the large scales to the small scales until molecular viscous dissipation (forward-scatter), but the inverse transfer called backscatter in which energy is transferred from the small scales back to the large scales [52] is also in play, particularly for geophysical flows. This is explained by the relative dominance of the Coriolis force which creates vortical structures that appear two-dimensional. Historically, developing SGS models that account for backscatter is a challenging task [53–55]. Indeed, an overprediction of backscatter that can not be compensated by eddy-viscosity will lead to an accumulation of small-scale energy causing simulations to become numerically unstable. In two-dimensional flows, we observe a dual cascade composed of “forward” enstrophy and “inverse” energy, in a statistical sense. As a consequence, a large number of SGS models have been proposed in particular for geophysical flows (see [56] for a review) with well-documented configurations and performance metrics [57]. SGS modeling is also a key issue for the simulation of ocean and atmosphere dynamics because of the large range of motions involved [58–61]. As a case study framework, we consider barotropic QG flows. While providing an approximate yet representative system for rotating stratified flows found in the atmosphere and ocean dynamics, it involves relatively complex SGS features that make the learning problem non-trivial. As such, QG flows are regarded as an ideal playground to explore and assess the relevance of machine learning strategies for SGS models in geophysical turbulence. The governing equations of direct vorticity ω for the QG equations with

bottom topography η are

$$\frac{\partial \omega}{\partial t} + \mathcal{N}(\omega + \eta, \psi) = \nu \nabla^2 \omega - \mu \omega - \beta \partial_x \psi + F_{\omega}, \quad (26)$$

$$\nabla^2 \psi = -\omega \quad (27)$$

where $\mathcal{N}(\omega + \eta, \psi) = \partial_x \psi \partial_y (\omega + \eta) - \partial_y \psi \partial_x (\omega + \psi)$ is the non-linear vorticity advection, ν is the viscosity, μ is a large-scale drag coefficient, β is the Earth rotation vector approximation by beta-plane and F_{ω} is an additional source term. Now, the derivation of the reduced system for QG dynamics follows the same procedure that is typically used for fluid dynamics turbulence modeling (also called large-eddy simulation). The projection operator \mathcal{T} at spatial coordinate \mathbf{x} is here given as a discretization (or coarse-graining) $\mathcal{D} : \Omega \rightarrow \bar{\Omega}$ and the convolution of ω with a kernel function $G(\mathbf{x})$ [62],

$$\bar{\omega}(\mathbf{x}) = \mathcal{D} \left(\int G(\mathbf{x} - \mathbf{x}') \omega(\mathbf{x}') d\mathbf{x}' \right). \quad (28)$$

We can then derive the equations which govern the evolution of reduced vorticity $\bar{\omega}$,

$$\begin{aligned} \frac{\partial \bar{\omega}}{\partial t} + \mathcal{N}(\bar{\omega} + \bar{\eta}, \bar{\psi}) = \nu \nabla^2 \bar{\omega} - \mu \bar{\omega} - \beta \partial_x \bar{\psi} + \bar{F}_{\omega} \\ + \underbrace{\mathcal{N}(\bar{\omega} + \bar{\eta}, \bar{\psi}) - \overline{\mathcal{N}(\omega + \eta, \psi)}}_{\tau_{\omega}} \end{aligned} \quad (29)$$

where τ_{ω} is the SGS term. In this context, τ_{ω} can not be determined from the reduced variables because of the non-linear interactions of small-scale dynamics $\mathcal{N}(\omega + \eta, \psi)$ and must thus be statistically modeled in order to close equation (29).

IV.1. Simulation setup

In order to study the learning problem, we solve equations (26)–(27) using a pseudospectral code with full 3/2 dealiasing [63] and a classical fourth-order explicit Runge Kutta time advancement. The system is defined in a squared domain $\Omega, \bar{\Omega} \in [-\pi, \pi]^2$, or domain length $L = 2\pi$ discretized with a Fourier basis, i.e. double-periodic boundary conditions on N and \bar{N} grid points with uniform spacing and a grid ratio $\Delta' = N/\bar{N} > 1$ between direct and reduced solver resolutions. We extract the SGS term with spatial filtering (28) using a spectral cut-off filter G and sample non-residual quantities along the simulations, i.e. $\{\omega \rightarrow \tau_{\omega}\}$ is obtained from direct solver f and $\{\bar{\omega}\}$ is obtained from reduced solver g . We energize the system using a wind-forced configuration representative of mesoscale oceanic simulation [64]. We produce an equilibrium solution from a slowly varying in time circular source at large scale k with steady enstrophy rate injection $\langle F_{\omega}(t)^2 \rangle = 3$ such that

$$F_{\omega}(t) = \cos(4y) - \cos(4x + \pi \sin(1.5t)). \quad (30)$$

Algorithm 1 Two-step online SGS learning algorithm

```

input:  $\{\bar{\mathbf{y}}(t)\}_{t \in [t_0, t_1]}$  // PRECOMPUTED USING REDUCED SOLVER  $g$ 
input:  $\{\mathbf{y}(t), \tau(\mathbf{y}(t))\}_{t \in [t_0, t_1]}$  // PRECOMPUTED USING DIRECT SOLVER  $f$ 
input:  $\mathcal{E}(\Theta \sim \mathcal{N})$  // DEFINED EMULATOR NN ARCHITECTURE
input:  $\mathcal{M}(\theta \sim \mathcal{N})$  // DEFINED MODEL NN ARCHITECTURE
output:  $\mathcal{M}(\theta)$  // OPTIMIZED SGS PARAMETERS  $\theta$ 
 $\mathcal{M}(\theta) \leftarrow \text{MODEL\_STEP}(\mathcal{E}(\Theta) \leftarrow \text{EMULATOR\_STEP})$  // LEARN  $\mathcal{M}$  FROM THE TRAINED EMULATOR  $\mathcal{E}$ 

function EMULATOR\_STEP
  while Not converged do // RUN EPOCHS UNTIL CONVERGENCE
    for  $t \leftarrow t_0, t_1$  do
       $\hat{\mathbf{y}}(t) \leftarrow \bar{\mathbf{y}}(t)$  // INITIALIZE FROM REDUCED STATES  $\bar{\mathbf{y}}$ 
      for  $i \leftarrow 0, N_{\text{steps}}$  do // LOOP OVER TEMPORAL HORIZON
         $\hat{\mathbf{y}}(t + (i + 1)\delta t) \leftarrow \text{ODE}(\mathcal{E}(\hat{\mathbf{y}}(t + i\delta t) | \Theta))$  // INTEGRATE USING ODE SOLVER
      end for
       $\mathcal{L}_{>}^{\mathcal{E}} \leftarrow \ell_{>}^{\mathcal{E}}(\{\bar{\mathbf{y}}(t + i\delta t)\}_{i \in [1, M]}, \{\hat{\mathbf{y}}(t + i\delta t)\}_{i \in [1, M]})$  // CLASSICAL "ONLINE" LOSS
       $\nabla_{\Theta} \mathcal{L}_{>}^{\mathcal{E}} \leftarrow \text{BACKPROP}(\mathcal{L}_{>}^{\mathcal{E}})$  // COMPUTE GRADIENT OF DIFFERENTIABLE LOSS  $\ell_{>}^{\mathcal{E}}$ 
       $\Theta \leftarrow \text{OPTIMIZE}(\nabla_{\Theta} \mathcal{L}_{>}^{\mathcal{E}})$  // APPLY GRADIENT DESCENT
    end for
  end while
end function

function MODEL\_STEP( $\mathcal{E}(\Theta)$ )
  while Not converged do // RUN EPOCHS UNTIL CONVERGENCE
    for  $t \leftarrow t_0, t_1$  do
       $\hat{\mathbf{y}}(t) \leftarrow \mathcal{T}(\mathbf{y}(t))$  // INITIALIZE FROM PROJECTED DIRECT STATES  $\mathbf{y}$ 
      for  $i \leftarrow 0, N_{\text{steps}}$  do // LOOP OVER TEMPORAL HORIZON
         $\hat{\mathbf{y}}(t + (i + 1)\delta t) \leftarrow \text{ODE}(\mathcal{E}(\hat{\mathbf{y}}(t + i\delta t)) + \mathcal{M}(\hat{\mathbf{y}}(t + i\delta t) | \theta))$  // INTEGRATE USING ODE SOLVER
      end for
       $\mathcal{L}_{>}^{\mathcal{M}_c} \leftarrow \ell_{>}^{\mathcal{M}_c}(\{\tau(\mathbf{y}(t + i\delta t))\}_{i \in [1, M]}, \{\mathcal{M}(\hat{\mathbf{y}}(t + i\delta t) | \theta)\}_{i \in [1, M]})$  // TEMPORAL "OFFLINE" LOSS
       $\nabla_{\theta} \mathcal{L}_{>}^{\mathcal{M}_c} \leftarrow \text{BACKPROP}(\mathcal{L}_{>}^{\mathcal{M}_c})$  // COMPUTE GRADIENT OF COMPENSATED LOSS  $\ell_{>}^{\mathcal{M}_c}$ 
       $\theta \leftarrow \text{OPTIMIZE}(\nabla_{\theta} \mathcal{L}_{>}^{\mathcal{M}_c})$  // APPLY GRADIENT DESCENT
    end for
  end while
end function

```

We also use unaligned sinusoidal bumps topography [65] in order to create interesting dynamics with significant nonzonal components in jets induced by the Coriolis force. Stationary turbulent states are obtained from random Gaussian initialization $\omega(t = 0) \sim \mathcal{N}(0, 1)$ at moderate wavenumbers $k \in [10, 32]$, followed by a 500000 iterations spin-up on a smaller grid (1024^2) and energy propagation to the smallest scales of the direct grid (2048^2) in about 25000 iterations. We show examples of vorticity fields and SGS term in Fig. 1.

IV.2. Learning setup

To generate the corresponding datasets suitable for online learning, we need continuous trajectories and thus subsample at each iteration from g for (17) and one state every Δ' iteration performed by f for (18) so that these states directly correspond to one iteration performed by g . For the SGS model, we use a simple standard CNN with $D = 10$ convolution layers with kernels K of size 5 and 64 filters each, followed by non-linear Relu acti-

vations. This architecture has been shown to be able to learn extremely accurate SGS dynamics in [20]. For the large-scale dynamics represented by the neural emulator \mathcal{E} , we explore a state-of-the-art neural architecture and a simpler CNN in order to assess the impact of the emulation quality on the SGS learning:

- **Dilated Residual Network (DRN).** The architecture combines residual networks with the encode-process-decode paradigm [66] and dilated convolutions, recently applied to different types of flows [67].

- **Convolutional Neural Network (CNN).** The architecture is equivalent to the CNN used for the SGS model except that we use $D = 7$ convolution layers.

Note that for each of these architectures, input boundaries are replicated periodically given the geometry of the domain. More involved architecture could further improve the overall performance and might be interesting to explore. However, we may point out that the goal is not to design an optimal NN-based architecture but

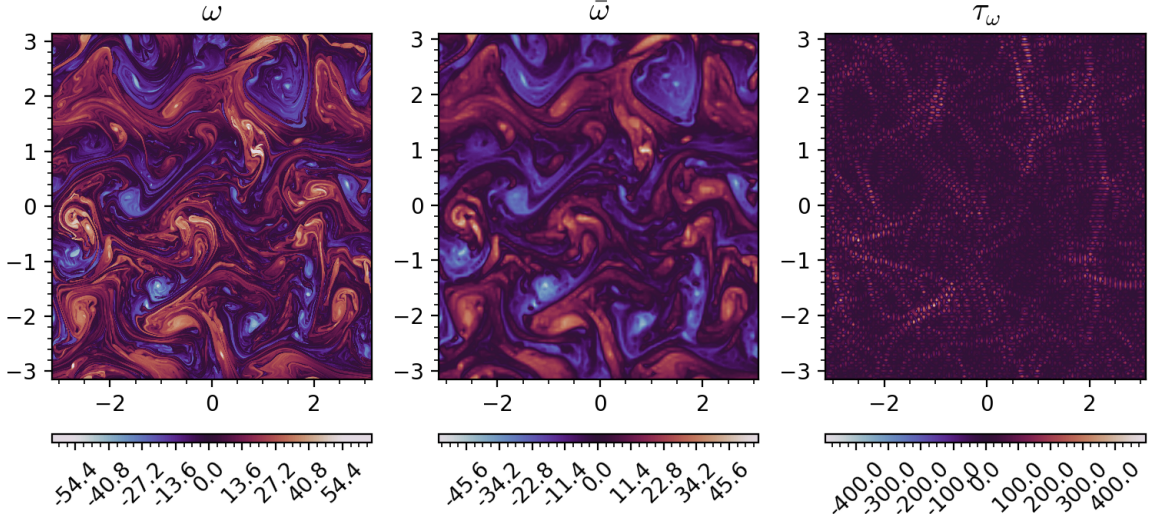


FIG. 1. Direct vorticity fields ω (left), reduced vorticity fields $\bar{\omega}$ (middle) and SGS term τ_ω (right) at the end of a testing horizon (3000 temporal iterations) from the direct simulation using f .

rather to evaluate the training strategy at the same SGS computational cost during evaluation stage. Concerning the functional loss ℓ , we restricted ourselves to simple MSE both for the neural emulator and the SGS model,

$$\ell_{<}(\cdot, \cdot) = \ell_{>}^{\mathcal{E}}(\cdot, \cdot) = \ell_{>}^{\mathcal{M}_c}(\cdot, \cdot) = \frac{1}{M} \sum_{i=1}^M \|\cdot_i - \hat{\cdot}_i\|_2^2. \quad (31)$$

V. RESULTS

We generate simulation data and train corresponding models using parameters summarized in Table. I. The objective here being to design a stable and efficient SGS model, we compare the results of our two-step algorithm with several baselines.

Online model (reference). The main objective here is to reproduce the performance of the online model implemented using a differentiable solver using our two-step strategy that does not require differentiability.

Offline model. We train a SGS model using the classical offline strategy with the same CNN architecture, as described above. This model is known to be unstable and motivates the advantages of the online strategy.

Physical model. As a common baseline, we also use the Smagorinsky model [68], defined as an eddy coefficient proportional to the resolved strain rate \bar{S} with the dynamic procedure proposed by [69, 70] to compute C_s and apply spatial averaging with positive clipping [50, 71] in order to avoid locally negative constants $C_s(x, y) < 0$, i.e. ensuring that the models are purely diffusive and $\nu_e \geq 0$,

$$\tau_\omega = \nabla \cdot \underbrace{[(C_s \Delta)^2 |\bar{S}|] \nabla \bar{\omega}}_{\nu_e}. \quad (32)$$

TABLE I. Parameters of the numerical setup for simulation (top) and learning (bottom). Note that reduced systems use the same parameters, except for grid resolution \bar{N} and timestep $\bar{\Delta t}$, obtained from the grid ratio Δ' . The quantities are given in numerical (dimensionless) as directly used in the solver for reproducibility.

Simulation parameter	
Length of the domain	$L = 2\pi$
Linear drag	$\mu = 2 \times 10^{-2}$
Kinematic viscosity	$\nu = 1.025 \times 10^{-5}$
Rossby parameter	$\beta = 2.195 \times 10^2$
Topography	$\eta = \sin(3y) + \cos(3x)$
Timestep	$\Delta t = 10^{-4}$
Number of grid points	$N = 2048$
Grid ratio	$\Delta' = 16$
Learning parameter	
offline batch size / online iterations	$M = 25$
Training trajectories	10
Testing trajectories	5
Samples per trajectory	3000

V.1. SGS model evaluation

We first run a new simulation from different random initial conditions with our references, baselines and SGS models trained using the two-step algorithm using both the CNN and DRN architectures. Recall that evaluations are now run with the reduced solver g and a SGS model \mathcal{M} , except for the direct reference \mathcal{M}_{DNS} that uses direct solver f .

We show in Fig. 2 the final vorticity fields $\bar{\omega}$ after 500 reduced temporal iterations. It is first clear here that the

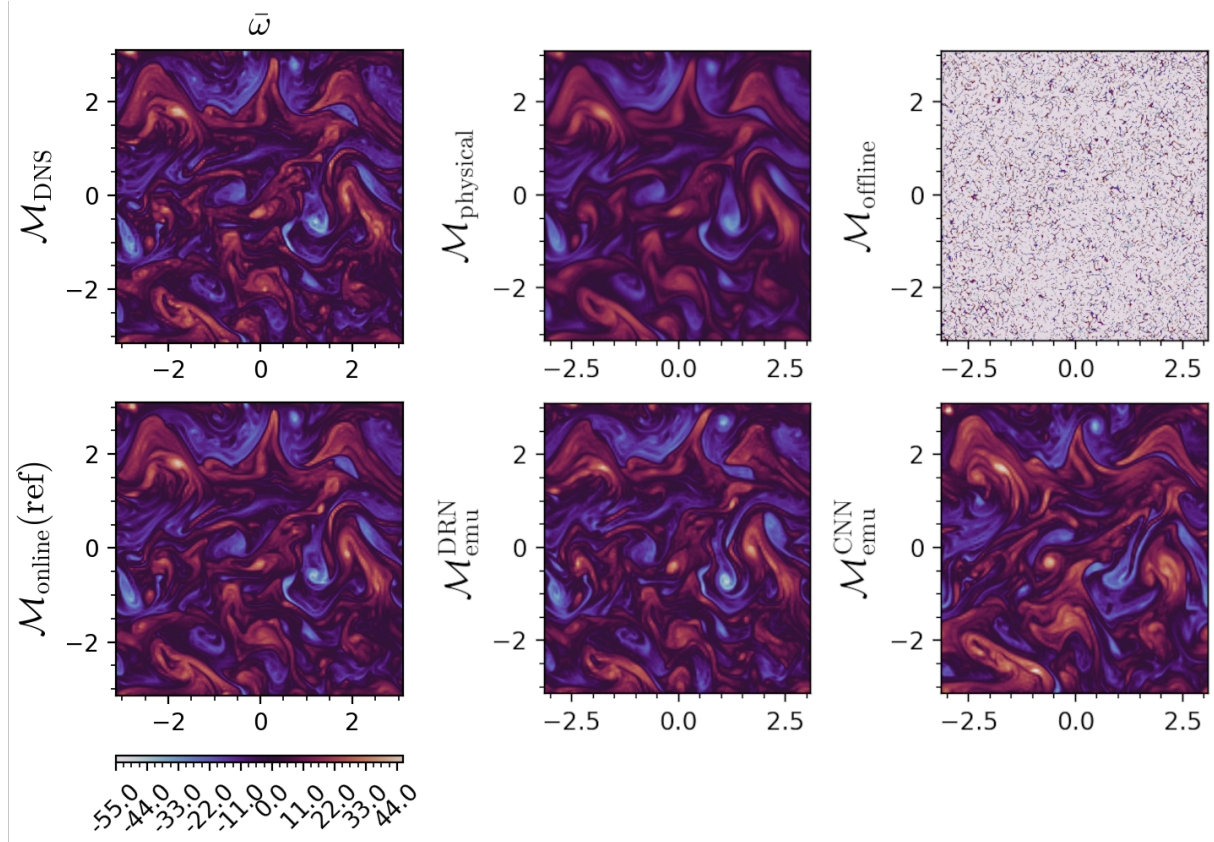


FIG. 2. Reduced vorticity fields $\bar{\omega}$ after a short simulation run of 500 temporal iterations comparing reference filtered DNS (top-left) and differentiable online strategy (bottom-left) with baselines (top-middle,right) and emulation-based models (bottom-middle,right).

offline learning strategy does not lead to a stable model in this configuration, and that numerical blowup characterized by a point-by-point noisy vorticity field happens quickly. On the opposite, the physical model is too diffusive, completely removing small-scale features and the associated dynamics.

We can also validate that the online strategy is indeed a stable and accurate model to represents the SGS dynamics in QG systems, as it is remarkably close to the DNS.

Concerning the neural emulators, they both remain stable over this temporal horizon. However, we can already see that model trained from the simpler CNN is already starting to differ from the reference.

To understand the time-evolution of the flow statistics, we look at the invariants of the QG equations in Fig. 3, in the limit of inviscid flows [72] for energy

$$E(t) = \frac{1}{2} \int \mathbf{u}(t)^2 \, dr \quad (33)$$

and enstrophy

$$Z(t) = \frac{1}{2} \int \omega(t)^2 \, dr. \quad (34)$$

We can confirm previous observations concerning accumulation of enstrophy from the offline model, exponentially growing until blowup. We also clearly observe the over-dissipation of enstrophy for the physical model. Both neural emulators show enstrophy evolution relatively close to the references with DNN-based model being almost equivalent to the reference online model. While small scales are well represented by the models trained from the neural emulators, it is apparent that they are not as efficient on the large scales, as seen by the constant increase of energy for the CNN-based model. The DNN-based model does not accumulate energy but performs slightly worse than the physical model.

Integrating over a longer temporal horizon composed of 3000 iterations, we can inspect the statistical behavior of the different models in Fig. 4. First, we verify that the enstrophy spectrum

$$Z(k) = \int_{|\mathbf{k}|=k} |\omega(\mathbf{k})|^2 \, dS(\mathbf{k}). \quad (35)$$

and integrated modeled transfers

$$\int \bar{\omega} \tau_\omega \, dS = \int (\bar{\mathbf{u}} \bar{\omega} - \bar{\mathbf{u}} \bar{\omega}) \cdot \nabla \bar{\omega} \, dS = - \int T_Z \, dS. \quad (36)$$

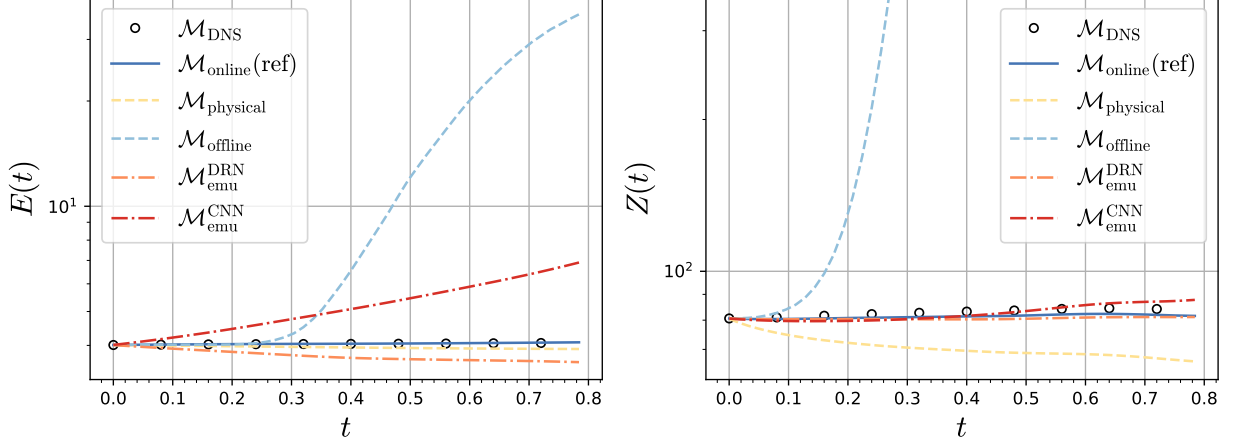


FIG. 3. Domain-averaged invariants energy $E(t)$ (left) and enstrophy $Z(t)$ (right) after a short simulation run of 500 temporal iterations.

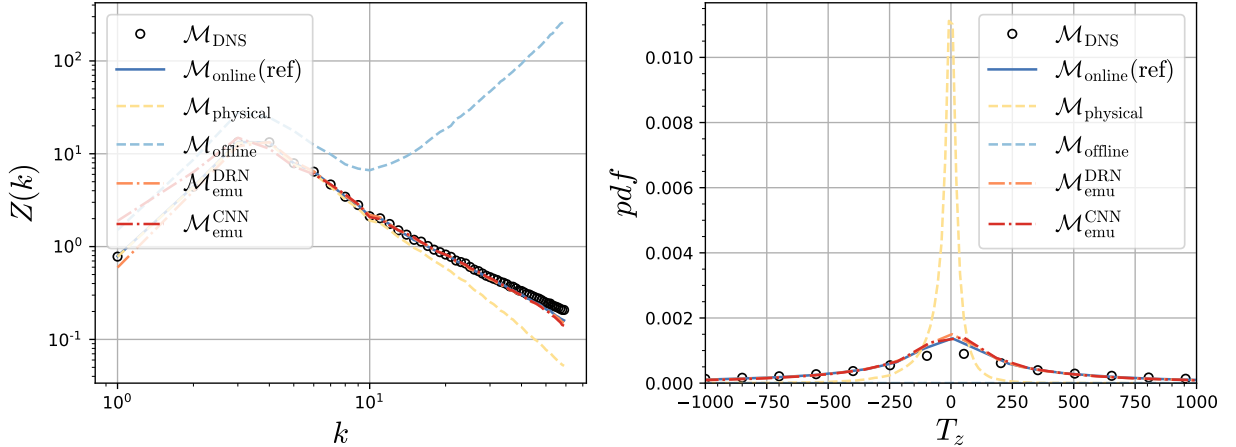


FIG. 4. Time-averaged enstrophy spectrum (left) and final probability distribution of the enstrophy transfer term (right) for 5 trajectories of longer simulation runs of 3000 temporal iterations.

of the online (differentiable reference) correctly reproduces the dynamics of the DNS. On the left, we note a good agreement of the physical model at the smallest wavenumbers but excessive dissipation at the largest wavenumbers. The DRN-based model is extremely accurate on the largest wavenumbers which corresponds with the terms used in the loss function during training, both ω and τ_ω acting mostly on the smallest scales. The DRN-based model is however not as accurate on the smallest wavenumbers. This might be improved by adding an additional large-scale term to the loss function such as velocity \mathbf{u} or streamfunction ψ . On the right, it is clear that the modeled transfers distribution produced by the physical model has a large peak and a poor reproduction of the distribution tails. On the other hand, the ML-based models are efficient at maintaining a modeled transfers distribution close to the references.

It is important to mention that experiments with SGS models trained from neural emulators with a state loss

$\ell^{\mathcal{M}} \equiv \ell^{\mathcal{E}}$ have been omitted from these plots because of their unstable behavior.

V.2. Neural emulator performance

We want here to identify the stability difference and better understand the source of error between models obtained from neural emulators of different complexities, mostly in terms of NN architecture and corresponding number of trainable parameters.

We look at the evolution of the root-mean-squared error (rms) of some reference \cdot and predicted $\hat{\cdot}$ quantities over temporal integration steps M ,

$$\ell_{\text{rms}}(\cdot, \hat{\cdot}) = \frac{1}{\sigma(\cdot)M} \sqrt{\frac{1}{N} \sum_{i=0}^N \|\cdot_i - \hat{\cdot}_i\|_2^2} \quad (37)$$

where σ is the standard deviation.

In Fig. 5, we show the ℓ_{rms} of different SGS models compared to the DNS. First, vorticity mismatch indicates that each model is able to improve substantially compared to the reduced simulation without SGS models (or \mathcal{M}_0). In particular, NN-based models produce an error that increases slower than the physical models. The emulator-based models are performing slightly worse than the reference online model but remain competitive. We also see that error for the offline approach grows linearly, while the other models follow a logarithmic shape. It may indicate that errors and instabilities develops after more than $M = 25$ temporal iterations. The velocity mismatch is quite different, since error for the CNN-based model grows faster and is already greater than the no model error. The error for the DRN-based model is still large compared to the other models, but also seems to grow linearly. It is clear here that there is still some progress to be made about the emulator-based predictions on the largest scales, potentially induced by some error bias in the neural emulator.

We isolate the error produced by the neural emulators compared to the solver a reduced resolution in Fig. 6. In addition to the neural emulators, we show the error produced by finite difference (FD) schemes (or emulators) of different orders from h^2 to h^6 using modified wavenumbers in a spectral method [73]. We can confirm that the error produced by the neural emulators is mainly affected by large scales. Indeed, the vorticity error of the DRN-based model is equivalent to a 6th order FD scheme, while the CNN-based model performs slightly worse than a 4th order FD but better than the 2nd order FD. However, both produce velocity errors larger than a 2nd order FD.

This further confirms that improvements on the large-scale predictions of the neural emulator are potentially a limitation that must be addressed.

VI. DISCUSSION

In this article, we have proposed an algorithm for training an online ML-based SGS parametrization, i.e., with *a posteriori* criteria for non-differentiable numerical solvers. The core idea of our approach is to use neural emulators that represent the reduced dynamics, equivalent to the original equations in a lower dimensional space. These emulators are by definition differentiable and allows us to train the parametrization in an online setting. The main benefit of our two-step algorithm is to avoid error compensation between the emulator and the trained ML-based parametrization using different loss targets for the SGS model and the neural emulator, respectively. Indeed, as demonstrated in section 3.2 above, learning jointly emulator and parametrization will lead to error compensation, where the parametrization-part accomodates the imperfect nature of the emulator-part. When used in a simulation, the trained parametrization is found to add spurious transfers that decreases overall performance. Our two-step algorithm has been tested

on a two-dimensional SGS modeling problem and shows performance levels close to those obtained with online learning on differentiable solvers. In a highly turbulent quasi-geostrophic setting with bottom topography, the model trained with our two-step algorithm is able to remain stable over many temporal iterations. Moreover, it has a matching performance with the online model in terms of small-scale quantities, and overall enstrophy spectrum and transfers distribution. Nonetheless, additional work will be required in order to alleviate some systematic biases in the SGS model associated with the inherently imperfect nature of the neural emulator. This error is mostly visible at large scale. We think that constraining the loss function of the neural emulator on related large scale quantities such as velocities instead of vorticity could further improve its performance, translating to a smaller bias in the learned SGS model.

This work represents a first step toward more complex neural emulators. While the experimental system used here has a considerable amount of state parameters, more work will still be required for deploying our approach with full complexity physical models. We have also seen that the SGS learning step is sensitive to the quality of the neural emulator, which could be a potential issue when emulating larger numerical systems. At this stage, it is also unclear how our algorithm compares with other existing gradient free training techniques and a systematic inter-comparison in terms of cost and performance would be needed. We note that the neural emulator approach is not only relevant for SGS parametrization but also more generally for differentiable computing, with a large potential in Earth System Modeling [31]. Our emulation-based approach could be leveraged for other task as for instance for calibrating model parameters [32] or learning model error [74]. Our algorithm could also provide a practical solution for deploying variational data assimilation (DA) techniques without having to compute the adjoint of the direct solver [75]. In practice, variational DA frameworks requires an adjoint operator which is complicated to maintain. Adjoint-free minimization techniques have been proposed, including ensemble methods [76] but trades-off performance and computing time. In previous work [45] and recent applications to different tasks, differentiable emulation opens a possible alternative approach for variational DA of numerical models.

It is important to mention that building a neural emulator for a specific problem can be done using different quantities. Here, we used the neural emulator to predict the model state-space evolution (or right-hand-side) of the dynamical system, which allows us to learn on different temporal horizons. It is also possible to use neural emulation to map model states at different future times in order to train SGS parametrizations [77].

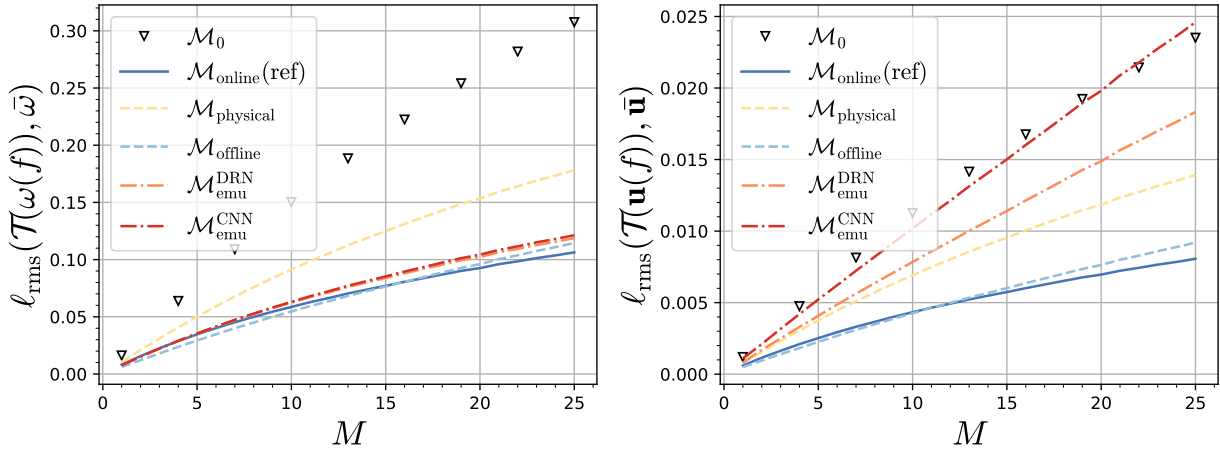


FIG. 5. ℓ_{rms} normalized by the number of temporal integration steps M for the vorticity ω (left) and velocity \mathbf{u} (right). The error for each SGS model is computed w.r.t. the DNS. As for comparison, we also show the reduced simulation without model (\mathcal{M}_0) that is known to be unstable.

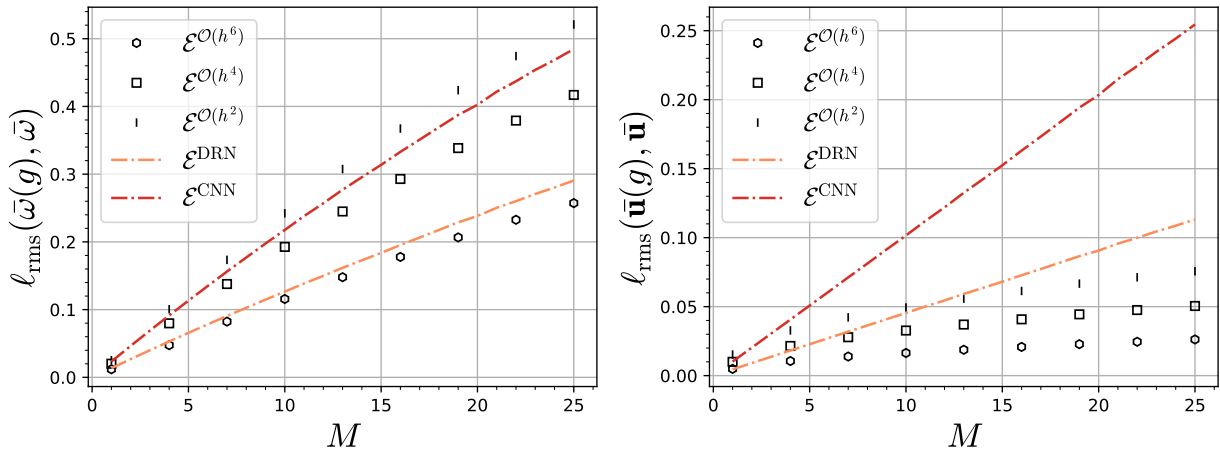


FIG. 6. ℓ_{rms} w.r.t. the reduced DNS, normalized by the number of temporal integration steps M for the reduced vorticity $\bar{\omega}$ (left) and velocity $\bar{\mathbf{u}}$ (right) for NN-based emulators and finite difference discretization of different orders.

ACKNOWLEDGMENTS

This research was supported by the CNRS through the 80 PRIME project, the ANR through the Melody, OceaniX. As part of the M2LiNES project, additional

support was also provided by Schmidt Futures, a philanthropic initiative founded by Eric and Wendy Schmidt, as part of its Virtual Earth System Research Institute (VESRI). Computations were performed using GPU resources from GENCI-IDRIS.

[1] R. S. Rogallo and P. Moin, Numerical simulation of turbulent flows, *Annual Review of Fluid Mechanics* **16**, 99 (1984).

[2] C. Meneveau and J. Katz, Scale-invariance and turbulence models for large-eddy simulation, *Annual Review of Fluid Mechanics* **32**, 1 (2000).

[3] B. Fox-Kemper, A. Adcroft, C. W. Böning, E. P. Chassignet, E. Curchitser, G. Danabasoglu, C. Eden, M. H. England, R. Gerdes, R. J. Greatbatch, *et al.*, Challenges and prospects in ocean circulation models, *Frontiers in Marine Science* **6**, 65 (2019).

[4] T. Schneider, S. Lan, A. Stuart, and J. Teixeira, Earth system modeling 2.0: A blueprint for models that learn from observations and targeted high-resolution simulations, *Geophysical Research Letters* **44**, 12 (2017).

[5] P. Maher, G. K. Vallis, S. C. Sherwood, M. J. Webb, and P. G. Sansom, The impact of parameterized convection on climatological precipitation in atmospheric global climate models, *Geophysical Research Letters* **45**, 3728 (2018).

[6] H. T. Hewitt, M. Roberts, P. Mathiot, A. Biastoch, E. Blockley, E. P. Chassignet, B. Fox-Kemper, P. Hyder, D. P. Marshall, E. Popova, *et al.*, Resolving and parameterising the ocean mesoscale in earth system models, *Current Climate Change Reports* **6**, 137 (2020).

[7] S. L. Brunton, B. R. Noack, and P. Koumoutsakos, Machine learning for fluid mechanics, *Annual Review of Fluid Mechanics* **52**, 477 (2020).

[8] R. Vinuesa and S. L. Brunton, Enhancing computational fluid dynamics with machine learning, *Nature Computational Science* **2**, 358 (2022).

[9] T. Arcomano, I. Szunyogh, A. Wikner, J. Pathak, B. R. Hunt, and E. Ott, A hybrid approach to atmospheric modeling that combines machine learning with a physics-based numerical model, *Journal of Advances in Modeling Earth Systems* **14**, e2021MS002712 (2022).

[10] M. Sonnewald, R. Lguensat, D. C. Jones, P. D. Dueben, J. Brajard, and V. Balaji, Bridging observations, theory and numerical simulation of the ocean using machine learning, *Environmental Research Letters* **16**, 073008 (2021).

[11] P. I. Karpov, C. Huang, I. Sitzdikov, C. L. Fryer, S. Woosley, and G. Pilania, Physics-informed machine learning for modeling turbulence in supernovae, *The Astrophysical Journal* **940**, 26 (2022).

[12] S. Pawar, O. San, A. Rasheed, and P. Vedula, Frame invariant neural network closures for Kraichnan turbulence, *Physica A: Statistical Mechanics and its Applications* **609**, 128327 (2023).

[13] H. Frezat, G. Balarac, J. Le Sommer, R. Fablet, and R. Lguensat, Physical invariance in neural networks for subgrid-scale scalar flux modeling, *Physical Review Fluids* **6**, 024607 (2021).

[14] T. Beucler, M. Pritchard, S. Rasp, J. Ott, P. Baldi, and P. Gentine, Enforcing analytic constraints in neural networks emulating physical systems, *Physical Review Letters* **126**, 098302 (2021).

[15] H. A. Pahlavan, P. Hassanzadeh, and M. J. Alexander, Explainable offline-online training of neural networks for parameterizations: A 1d gravity wave-QBO testbed in the small-data regime, arXiv preprint [10.48550/arXiv.2309.09024](https://arxiv.org/abs/2309.09024) (2023).

[16] J. Sirignano and J. F. MacArt, Dynamic deep learning closures: Online optimization with embedded DNS, arXiv preprint [10.48550/arXiv:2303.02338](https://arxiv.org/abs/2303.02338) (2023).

[17] J. Sirignano, J. F. MacArt, and J. B. Freund, DPM: A deep learning PDE augmentation method with application to large-eddy simulation, *Journal of Computational Physics* **423**, 109811 (2020).

[18] K. Duraisamy, Perspectives on machine learning-augmented Reynolds-averaged and large eddy simulation models of turbulence, *Physical Review Fluids* **6**, 050504 (2021).

[19] J. F. MacArt, J. Sirignano, and J. B. Freund, Embedded training of neural-network subgrid-scale turbulence models, *Physical Review Fluids* **6**, 050502 (2021).

[20] H. Frezat, J. Le Sommer, R. Fablet, G. Balarac, and R. Lguensat, A posteriori learning for quasi-geostrophic turbulence parametrization, *Journal of Advances in Modeling Earth Systems* **14**, e2022MS003124 (2022).

[21] B. List, L.-W. Chen, and N. Thuerey, Learned turbulence modelling with differentiable fluid solvers: physics-based loss functions and optimisation horizons, *Journal of Fluid Mechanics* **949**, A25 (2022).

[22] X. Fan and J.-X. Wang, Differentiable hybrid neural modeling for fluid-structure interaction, arXiv preprint [10.48550/arXiv.2303.12971](https://arxiv.org/abs/2303.12971) (2023).

[23] V. Shankar, V. Puri, R. Balakrishnan, R. Maulik, and V. Viswanathan, Differentiable physics-enabled closure modeling for Burgers' turbulence, *Machine Learning: Science and Technology* **4**, 015017 (2023).

[24] K. Um, R. Brand, Y. R. Fei, P. Holl, and N. Thuerey, Solver-in-the-loop: Learning from differentiable physics to interact with iterative PDE-solvers, in *Advances in Neural Information Processing Systems*, Vol. 33 (2020) pp. 6111–6122.

[25] P. Holl, V. Koltun, and N. Thuerey, Learning to control PDEs with differentiable physics, arXiv preprint [10.48550/arXiv.2001.07457](https://arxiv.org/abs/2001.07457) (2020).

[26] E. Heiden, D. Millard, E. Coumans, Y. Sheng, and G. S. Sukhatme, NeuralSim: Augmenting differentiable simulators with neural networks, in *2021 IEEE International Conference on Robotics and Automation (ICRA)* (IEEE, 2021) pp. 9474–9481.

[27] G. Négier, M. W. Mahoney, and A. S. Krishnapriyan, Learning differentiable solvers for systems with hard constraints, arXiv preprint [10.48550/arXiv.2207.08675](https://arxiv.org/abs/2207.08675) (2022).

[28] G. Dresdner, D. Kochkov, P. Norgaard, L. Zepeda-Núñez, J. A. Smith, M. P. Brenner, and S. Hoyer, Learning to correct spectral methods for simulating turbulent flows, arXiv preprint [10.48550/arXiv.2207.00556](https://arxiv.org/abs/2207.00556) (2022).

[29] D. Kochkov, J. A. Smith, A. Alieva, Q. Wang, M. P. Brenner, and S. Hoyer, Machine learning-accelerated computational fluid dynamics, *Proceedings of the National Academy of Sciences* **118**, e2101784118 (2021).

[30] T. Takahashi, J. Liang, Y.-L. Qiao, and M. C. Lin, Differentiable fluids with solid coupling for learning and control, in *Proceedings of the AAAI Conference on Artificial Intelligence*, Vol. 35 (2021) pp. 6138–6146.

[31] M. Gelbrecht, A. White, S. Bathiany, and N. Boers, Differentiable programming for earth system modeling, *Geoscientific Model Development* **16**, 3123 (2023).

[32] G. L. Wagner, A. Hillier, N. C. Constantinou, S. Silvestri, A. Souza, K. Burns, A. Ramadhan, C. Hill, J.-M. Campin, J. Marshall, *et al.*, CATKE: a turbulent-kinetic-energy-based parameterization for ocean micro-turbulence with dynamic convective adjustment, arXiv preprint [10.48550/arXiv.2306.13204](https://arxiv.org/abs/2306.13204) (2023).

[33] A. Ramadhan, J. Marshall, A. Souza, G. L. Wagner, M. Ponnappati, and C. Rackauckas, Capturing missing physics in climate model parameterizations using neural differential equations, arXiv preprint [10.48550/arXiv.2010.12559](https://arxiv.org/abs/2010.12559) (2020).

[34] S. Pawar and O. San, Data assimilation empowered neural network parametrizations for subgrid processes in geophysical flows, *Physical Review Fluids* **6**, 050501 (2021).

[35] D. Z. Huang, J. Huang, S. Reich, and A. M. Stuart, Efficient derivative-free Bayesian inference for large-scale inverse problems, *Inverse Problems* **38**, 125006 (2022).

[36] M. A. Iglesias, K. J. Law, and A. M. Stuart, Ensemble Kalman methods for inverse problems, *Inverse Problems* **29**, 045001 (2013).

[37] N. B. Kovachki and A. M. Stuart, Ensemble Kalman inversion: a derivative-free technique for machine learning tasks, *Inverse Problems* **35**, 095005 (2019).

[38] I. Lopez-Gomez, C. Christopoulos, H. L. Langendijk, Ervik, O. R. Dunbar, Y. Cohen, and T. Schnei-

der, Training physics-based machine-learning parameterizations with gradient-free ensemble kalman methods, *Journal of Advances in Modeling Earth Systems* **14**, e2022MS003105 (2022).

[39] J. Kim, H. Kim, J. Kim, and C. Lee, Deep reinforcement learning for large-eddy simulation modeling in wall-bounded turbulence, *Physics of Fluids* **34** (2022).

[40] M. Kurz, P. Offenhäuser, and A. Beck, Deep reinforcement learning for turbulence modeling in large eddy simulations, *International Journal of Heat and Fluid Flow* **99**, 109094 (2023).

[41] G. Novati, H. L. de Laroussilhe, and P. Koumoutsakos, Automating turbulence modelling by multi-agent reinforcement learning, *Nature Machine Intelligence* **3**, 87 (2021).

[42] H. J. Bae and P. Koumoutsakos, Scientific multi-agent reinforcement learning for wall-models of turbulent flows, *Nature Communications* **13**, 1443 (2022).

[43] K. Cranmer, J. Brehmer, and G. Louppe, The frontier of simulation-based inference, *Proceedings of the National Academy of Sciences* **117**, 30055 (2020).

[44] M. Bocquet, Surrogate modeling for the climate sciences dynamics with machine learning and data assimilation, *Frontiers in Applied Mathematics and Statistics* **9**, 1133226 (2023).

[45] M. Nonnenmacher and D. S. Greenberg, Deep emulators for differentiation, forecasting, and parametrization in earth science simulators, *Journal of Advances in Modeling Earth Systems* **13**, e2021MS002554 (2021).

[46] A. G. Baydin, B. A. Pearlmutter, A. A. Radul, and J. M. Siskind, Automatic differentiation in machine learning: a survey, *Journal of Machine Learning Research* **18**, 1 (2018).

[47] S. Hochreiter, The vanishing gradient problem during learning recurrent neural nets and problem solutions, *International Journal of Uncertainty, Fuzziness and Knowledge-Based Systems* **6**, 107 (1998).

[48] P. Sagaut, *Large eddy simulation for incompressible flows: an introduction* (Springer Science & Business Media, 2005).

[49] R. Maulik, O. San, A. Rasheed, and P. Vedula, Subgrid modelling for two-dimensional turbulence using neural networks, *Journal of Fluid Mechanics* **858**, 122 (2019).

[50] Y. Guan, A. Chattopadhyay, A. Subel, and P. Hassanzadeh, Stable a posteriori les of 2d turbulence using convolutional neural networks: Backscattering analysis and generalization to higher re via transfer learning, *Journal of Computational Physics* **458**, 111090 (2022).

[51] Y. Guan, A. Subel, A. Chattopadhyay, and P. Hassanzadeh, Learning physics-constrained subgrid-scale closures in the small-data regime for stable and accurate les, *Physica D: Nonlinear Phenomena* **443**, 133568 (2023).

[52] M. Lesieur and O. Metais, New trends in large-eddy simulations of turbulence, *Annual Review of Fluid Mechanics* **28**, 45 (1996).

[53] U. Piomelli, W. H. Cabot, P. Moin, and S. Lee, Subgrid-scale backscatter in turbulent and transitional flows, *Physics of Fluids A: Fluid Dynamics* **3**, 1766 (1991).

[54] U. Schumann, Stochastic backscatter of turbulence energy and scalar variance by random subgrid-scale fluxes, *Proceedings of the Royal Society of London. Series A: Mathematical and Physical Sciences* **451**, 293 (1995).

[55] Y. Liu, L. Lu, L. Fang, and F. Gao, Modification of spalart-allmaras model with consideration of turbulence energy backscatter using velocity helicity, *Physics Letters A* **375**, 2377 (2011).

[56] S. Danilov, S. Juricke, A. Kutsenko, and M. Oliver, Toward consistent subgrid momentum closures in ocean models, *Energy Transfers in Atmosphere and Ocean* **145** (2019).

[57] J. P. Graham and T. Ringler, A framework for the evaluation of turbulence closures used in mesoscale ocean large-eddy simulations, *Ocean Modelling* **65**, 25 (2013).

[58] M. F. Jansen, I. M. Held, A. Adcroft, and R. Hallberg, Energy budget-based backscatter in an eddy permitting primitive equation model, *Ocean Modelling* **94**, 15 (2015).

[59] S. Juricke, S. Danilov, A. Kutsenko, and M. Oliver, Ocean kinetic energy backscatter parametrizations on unstructured grids: Impact on mesoscale turbulence in a channel, *Ocean Modelling* **138**, 51 (2019).

[60] S. Juricke, S. Danilov, N. Koldunov, M. Oliver, and D. Sidorenko, Ocean kinetic energy backscatter parametrization on unstructured grids: Impact on global eddy-permitting simulations, *Journal of Advances in Modeling Earth Systems* **12**, e2019MS001855 (2020).

[61] J. S. Frederiksen, T. J. O’Kane, and M. J. Zidikheri, Stochastic subgrid parameterizations for atmospheric and oceanic flows, *Physica Scripta* **85**, 068202 (2012).

[62] A. Leonard, Energy cascade in large-eddy simulations of turbulent fluid flows, in *Advances in Geophysics*, Vol. 18 (Elsevier, 1975) pp. 237–248.

[63] C. Canuto, M. Y. Hussaini, A. Quarteroni, and T. A. Zang, *Spectral methods: fundamentals in single domains* (Springer Science & Business Media, 2007).

[64] B. Fox-Kemper and D. Menemenlis, Can large eddy simulation techniques improve mesoscale rich ocean models?, *Washington DC American Geophysical Union Geophysical Monograph Series* **177**, 319 (2008).

[65] A. F. Thompson, Jet formation and evolution in baroclinic turbulence with simple topography, *Journal of Physical Oceanography* **40**, 257 (2010).

[66] A. Sanchez-Gonzalez, N. Heess, J. T. Springenberg, J. Merel, M. Riedmiller, R. Hadsell, and P. Battaglia, Graph networks as learnable physics engines for inference and control, in *International Conference on Machine Learning* (PMLR, 2018) pp. 4470–4479.

[67] K. Stachenfeld, D. B. Fielding, D. Kochkov, M. Cranmer, T. Pfaff, J. Godwin, C. Cui, S. Ho, P. Battaglia, and A. Sanchez-Gonzalez, Learned coarse models for efficient turbulence simulation, arXiv preprint [10.48550/arXiv.2112.15275](https://arxiv.org/abs/10.48550/arXiv.2112.15275) (2021).

[68] J. Smagorinsky, General circulation experiments with the primitive equations: I. the basic experiment, *Monthly Weather Review* **91**, 99 (1963).

[69] M. Germano, U. Piomelli, P. Moin, and W. H. Cabot, A dynamic subgrid-scale eddy viscosity model, *Physics of Fluids A: Fluid Dynamics* **3**, 1760 (1991).

[70] D. K. Lilly, A proposed modification of the germano subgrid-scale closure method, *Physics of Fluids A: Fluid Dynamics* **4**, 633 (1992).

[71] S. Pawar, O. San, A. Rasheed, and P. Vedula, A priori analysis on deep learning of subgrid-scale parameterizations for kraichnan turbulence, *Theoretical and Computational Fluid Dynamics* **34**, 429 (2020).

[72] F. Bouchet and A. Venaille, Statistical mechanics of two-dimensional and geophysical flows, *Physics Reports* **515**, 227 (2012).

- [73] A. Kravchenko and P. Moin, On the effect of numerical errors in large eddy simulations of turbulent flows, *Journal of Computational Physics* **131**, 310 (1997).
- [74] A. Farchi, P. Laloyaux, M. Bonavita, and M. Bocquet, Using machine learning to correct model error in data assimilation and forecast applications, *Quarterly Journal of the Royal Meteorological Society* **147**, 3067 (2021).
- [75] A. Carrassi, M. Bocquet, L. Bertino, and G. Evensen, Data assimilation in the geosciences: An overview of methods, issues, and perspectives, *Wiley Interdisciplinary Reviews: Climate Change* **9**, e535 (2018).
- [76] Y. Yang, C. Robinson, D. Heitz, and E. Mémin, Enhanced ensemble-based 4dvar scheme for data assimilation, *Computers & Fluids* **115**, 201 (2015).
- [77] C. Pedersen, L. Zanna, J. Bruna, and P. Perezhogin, Reliable coarse-grained turbulent simulations through combined offline learning and neural emulation, arXiv preprint [10.48550/arXiv.2307.13144](https://arxiv.org/abs/2307.13144) (2023).